Available online at www.sciencedirect.com
SCIENCE DIRECT®
Chemical Physics Letters 416 (2005) 152–159
CHEMICAL PHYSICS LETTERS
www.elsevier.com/locate/cplett

Water VUV electronic state spectroscopy by synchrotron radiation

R. Mota [a], R. Parafita [a], A. Giuliani [b,c], M.-J. Hubin-Franskin [c], J.M.C. Lourenço [d], G. Garcia [e], S.V. Hoffmann [f], N.J. Mason [g], P. A. Ribeiro [d], M. Raposo [d], P. Limão-Vieira [a,g,*]

[a] *Laboratório de Colisões Atómicas e Moleculares, Departamento de Física, CEFITEC, FCT-Universidade Nova de Lisboa, Quinta da Torre, P-2829-516 Caparica, Portugal*
[b] *Laboratoire de Spectrometrie de Masse, Institut de Chimie des Substances Naturelles, CNRS, Avenue de la Terrasse, F-91198, Gif-sur-Yvette Cedex, France*
[c] *Laboratoire de Spectroscopie d'Electrons Diffusés, Université de Liège, Institut de Chimie-Bât. B6C, B-4000 Liège, Belgium*
[d] *Grupo de Óptica e Imagem, Departamento de Física, CEFITEC, FCT-Universidade Nova de Lisboa, Quinta da Torre, 2829-516 Caparica, Portugal*
[e] *Instituto de Matemáticas y Física Fundamental, Consejo Superior de Investigaciones Científicas, Serrano 113-bis, 28006 Madrid, Spain*
[f] *Institute for Storage Ring Facilities, University of Aarhus, Ny Munkegade, DK-8000, Aarhus C, Denmark*
[g] *Centre of Molecular and Optical Sciences, Department of Physics and Astronomy, The Open University, Walton Hall, Milton Keynes MK7 6AA, UK*

Received 5 August 2005; in final form 17 September 2005
Available online 12 October 2005

Abstract

Electronic state spectroscopy of water has been studied using synchrotron radiation. The spectra presented in this Letter represent the highest resolution (~0.075 nm) measurements in the energy range 6.0–11.0 eV and have allowed a detailed analysis of several new vibrational progressions to be observed in the 8.5–10 eV region and enabled us to assign the Rydberg series in the 9.9–10.8 eV energy absorption for the first time. Absolute cross-sections are also reported and compared with the previous data.

1. Introduction

Water is the most abundant polyatomic molecule in the Universe, being detected in stellar and planetary atmospheres, comets and throughout the interstellar medium [1]. In the terrestrial atmosphere it is perhaps the most important greenhouse gas since it regulates the terrestrial atmosphere radiation balance [2]. Water is also the key component of all living organisms, playing an important role in the cellular environment as a universal solvent [3]. Our understanding of radiation damage within cells, and thence mutagenesis, depends upon the modelling of tracks through the cell, in turn depending upon our knowledge of collisional cross-sections with water and the nature of its electronic states and their dissociative pathways leading to the production of OH radicals [4–6]. The interaction of electrons with water molecules have recently been reviewed by Itikawa and Mason [7]; they reported that several questions remained as to the electronic state spectroscopy of water and a more detailed study of the electronic state spectroscopy of water would be beneficial.

Water has been the subject of several experimental and theoretical studies [8–19]. Absolute photo-absorption oscillator strengths for the valence shell of water have been reported by Chan et al. [20] from 6 to 200 eV. Photofragment fluorescence has been reported by Fillion et al. [21] in the energy range 10.9–12 eV. Diercksen et al. [22] report detailed theoretical studies on the complete dipole excitation and ionisation spectrum of H_2O, while Bursulaya et al. [15] reported a computer simulation of the H_2O 8 eV photo-absorption band under ambient and supercritical conditions. Recently, Tanaka and co-workers [23] have obtained by electron impact the fundamental mode dependence of water vibrational excitation in the 6–8 eV resonance region.

In this Letter, we report a detailed study of the electronic state spectroscopy of water using VUV photo-absorption. Since the photo-absorption cross-section is present on an absolute scale, the data may be used to model

* Corresponding author. Fax: +351 21 294 85 49.
E-mail address: plimaovieira@fct.unl.pt (P. Limão-Vieira).

0009-2614/$ - see front matter © 2005 Elsevier B.V. All rights reserved.
doi:10.1016/j.cplett.2005.09.073

and understand the absorption of radiation by H_2O in many different environments including atmospheric chemistry, radiation biology and astro-chemistry.

2. Structure and properties of H_2O

In its ground state water has C_{2v} symmetry, with three vibrational modes (υ_1, υ_2, υ_3) with excitation energies of 0.454, 0.198 and 0.466 eV, respectively: excitation of υ_1 corresponding to symmetric stretching, υ_2 to symmetric bending and υ_3 to anti-symmetric stretching, [24]. The electronic ground state valence configuration of water is $(1a_1)^2\ (2a_1)^2\ (1b_2)^2\ (3a_1)^2\ (1b_1)^2$:$\tilde{X}^1A_1$. The highest occupied molecular orbital is localized in the oxygen lone pair ($1b_1$) molecular orbital [25] and the VUV absorption spectrum is mainly attributable to the excitation from this MO [8]. According to Diercksen et al. [22], the outer valence region comprising ($1b_2$), ($3a_1$) and ($1b_1$) orbitals are largely nonbonding π_x, angular or torsional γ-bonding and O–H σ-bonding in character, respectively. However, Eland [25] reports some weakly O–H bonding character in the ($3a_1$) orbital. The lowest unoccupied molecular orbitals are the ($4a_1$)γ* and ($2b_2$)σ* valence-like [22].

Excitation of a $1b_1$ electron leads to excitation of Rydberg states converging to the ionic ground state with a bent geometry, whereas a promotion of a $3a_1$ electron to a Rydberg orbital forms a Rydberg series converging to the first ionic excited state with a quasi-linear geometry [21]. The lowest ionisation energy of H_2O, $^2B_1(1b_1^{-1})$, as recommended by Lias is (12.621 ± 0.002) eV [26]. The experimental vertical ionisation energy of $^2A_1(3a_1^{-1})$ has been obtained from [22] and is 14.73 eV.

3. Experimental procedure

The present high-resolution VUV photo-absorption measurements were made at the ASTRID synchrotron facility, University of Aarhus, Denmark. The experimental apparatus has been described in detail previously [27]. Synchrotron radiation passes through a static gas sample with a photomultiplier being used to measure the transmitted light intensity every 0.05 or 0.1 nm intervals (depending on the resolution required to resolve observed fine structure). The incident wavelength is selected using a toroidal dispersion grating with 2000 lines/mm. The experimental full-width half-maximum resolution for the present results is 0.075 nm, (corresponding to 3 meV) at the midpoint of the energy range studied. For wavelengths below 200 nm, a He gas flow is maintained through the small gap between the photomultiplier and the exit window of the gas cell, in order to prevent any absorption by air contributing to the spectrum. The range over which the data was recorded, 115–320 nm (10.8–3.9 eV), was determined by the transmission windows of the gas cell and the grating energy range, respectively. Although the present water VUV photo-absorption spectrum only exhibits absorption features for energies higher than 6.5 eV. The lithium fluoride entrance window also removes any higher order radiation entering the gas cell.

The sample pressure is measured by means of a baratron capacitance manometer. In order to ensure that the data was free of any saturation effects [27], the cross-section was measured over a wide pressure range, 0.020–1.090 Torr, with attenuations of less than 10%. The synchrotron beam ring current is monitored throughout the collection of each spectrum and the data corrected for any fluctuations in the incident radiation.

Absolute photo-absorption cross-sections are obtained using the Beer–Lambert attenuation law:

$$I_t = I_0 \exp(-n\sigma x),$$

where I_t is the radiation intensity transmitted through the gas sample, I_0 is that through an evacuated cell, n the molecular number density of the sample gas, σ the absolute photo-absorption cross-section, and x the absorption path length (25 cm). The accuracy of the cross-section is estimated to be ±5%.

The liquid sample was pure commercial deionised water. Samples were degassed by a repeated freeze–pump–thaw cycle.

4. Results

The absolute high resolution VUV photo-absorption spectrum of water is shown in Fig. 1 between 6.0 and 11.0 eV. Three absorption bands centred at 7.447, 9.672 and 10.011 eV may be identified as transitions from the $\tilde{X}^1A_1$ lowest neutral ground state to the $\tilde{A}^1B_1$, $\tilde{B}^1A_1$ and $\tilde{C}^1B_1$, respectively [8]; a fourth band centred at 10.163 eV has been identified as due to excitation of $\tilde{D}^1A_1 \leftarrow \tilde{X}^1A_1$ [15,20]. The first band is quite broad (Fig. 2) with only diffuse structure being observed (Table 1), the second (Fig. 3) and third (Fig. 4) bands are, in contrast, rich in structure, with their peak positions and assignments listed in Tables 2–4, respectively.

In contrast to many of the previous spectroscopic studies we have made absolute cross-section measurements. Earlier cross-section measurements of water vapour made by Watanabe and Jursa [9] at 10.783 eV (115 nm) report a value lower than 4.000 Mb in contrast to the present value of 4.828 Mb; the data from Gürtler et al. [12] and Yoshino et al. [14], in the energy range 6.841–9.852 eV (181.26–125.86 nm), are however, in good agreement with ours, within ±3%. The present cross-section to be of 5–10% higher than that by Chung et al. [16] and 10% lower than the result of Vatsa and Volpp [17] at the Lyman-α wavelength (121.567 nm), while the data from Lee and Suto [19] is ~8% higher than the present data. In the first absorption band between 6.5 and 6.8 eV, the present values are 7–15% higher than Parkinson and Yoshino [18]. We believe several of these differences may be attributed to the resolution of each of the apparatus and higher resolution leading to the observation of sharper structures and hence higher cross-sections; however, other factors, such as role of saturation

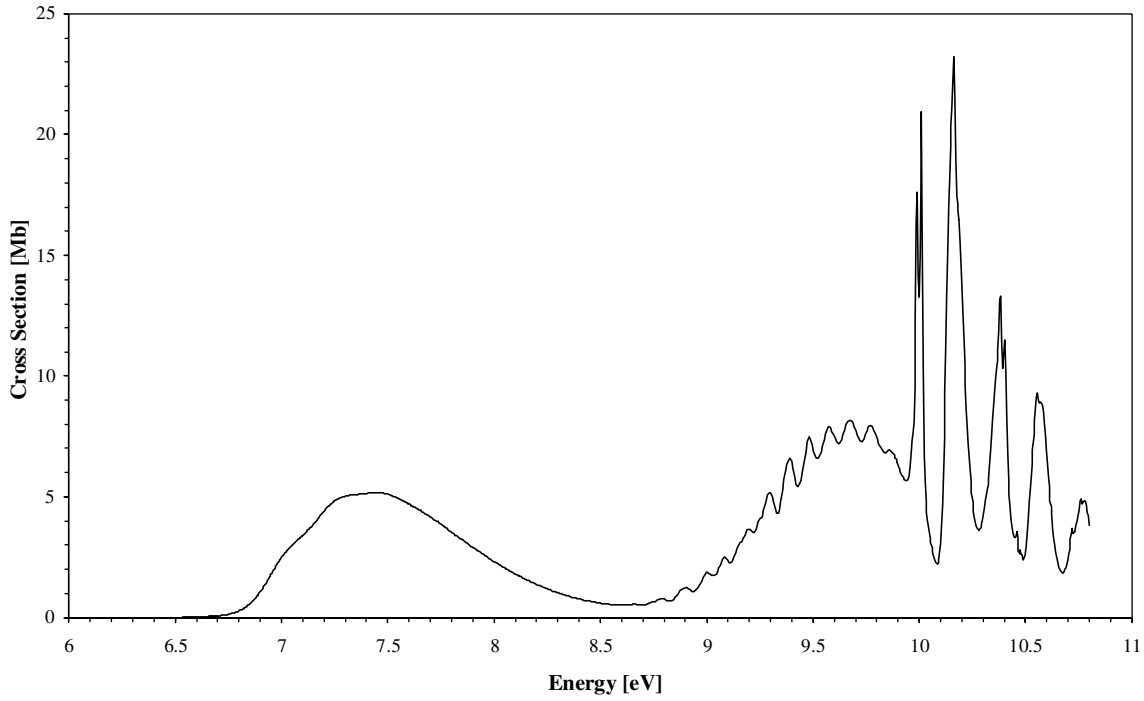

Fig. 1. VUV photo-absorption spectrum of H_2O in the 6.0–11.0 eV energy region.

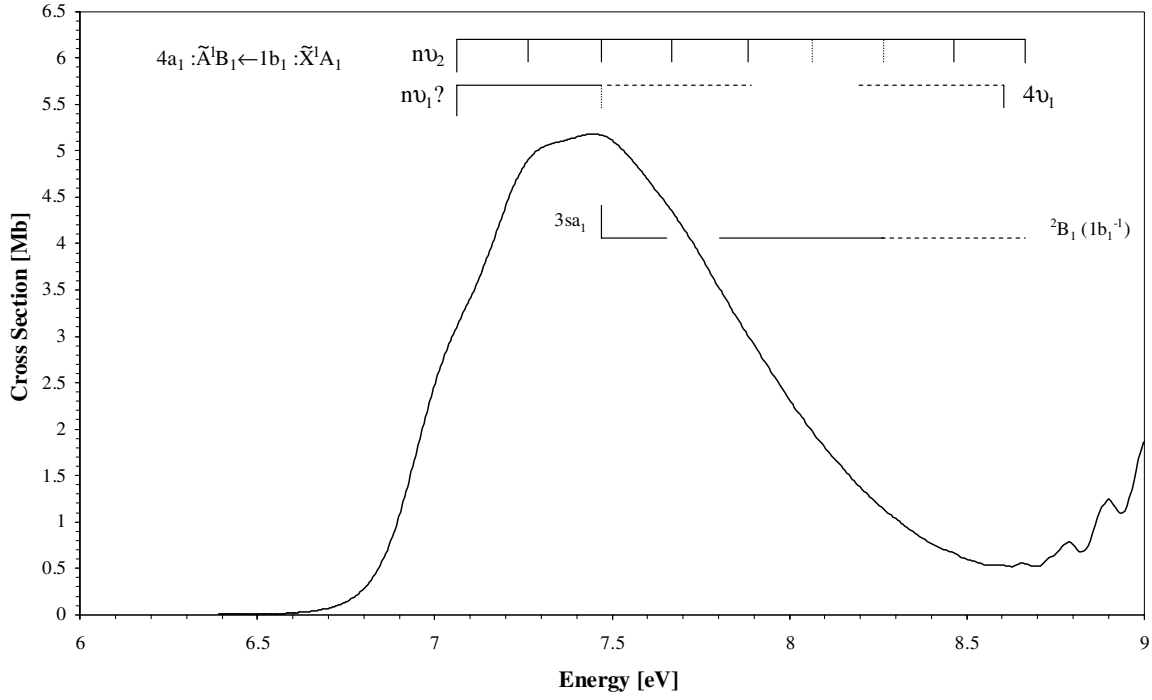

Fig. 2. H_2O photo-absorption spectrum from 6.0 to 9.0 eV with labelled vibrational series.

in other data sets may also lead to the observation of lower cross-sections by previous authors.

5. Discussion

The VUV spectrum has been measured previously, albeit with lower resolution, and a complete vibrational analyses of the bands lying at 9.999–10.973 and 9.920–12.400 eV has been made by Bell [10] and Price [8], respectively; Ishiguro et al. [13] reported the absorption spectra of H_2O and D_2O in the energy region 10.973–24.800 eV. In the following sections we will discuss each region in turn comparing our present results and assignments with those of earlier authors.

Table 1
Energy positions and vibrational analysis of features observed in the first absorption band (6.5–8.7 eV) of H_2O (energies in eV)

This work					Wang et al. [11]	
Energy	ΔE (υ_2')	Assignment	ΔE (υ_1')	Assignment	Energy	ΔE (υ_2')
7.069	–	υ_{00}	–	υ_{00}	7.022	–
7.263	0.194	$1\upsilon_2$	–	–	7.252	0.229
7.464	0.201	$2\upsilon_2$	0.395	$1\upsilon_1$	7.483	0.232
7.668	0.204	$3\upsilon_2$	–	–	7.712	0.228
7.872	0.204	$4\upsilon_2$	0.408	$2\upsilon_1$	–	–
8.067 (d)	0.195	$5\upsilon_2$	–	–	–	–
8.260 (d)	0.193	$6\upsilon_2$	0.388	$3\upsilon_1$	–	–
8.463	0.203	$7\upsilon_2$	–	–	–	–
8.604	–	–	0.344	$4\upsilon_1$		
8.658	0.195	$8\upsilon_2$	–	–	–	–

(d) means diffuse structure.

5.1. Valence excitation in the energy range 6.5–9.0 eV

Excitation in this energy region is a continuum, (Fig. 2 and Table 1) peaking at 7.447 eV (5.184 Mb). It corresponds to the first absorption band $4a_1 : \tilde{A}^1B_1 \leftarrow 1b_1 : \tilde{X}^1A_1$ of H_2O which has been shown to be dissociative on $OH(\tilde{X}^2\Pi) + H(^2S)$. The absorption however, superimposed upon it is a weak structure which may be ascribed to Rydberg character (see Section 5.4) [11,15]. The band also exhibits an extended poorly defined progression (seen here for the first time) which may be ascribed to the symmetric bending mode, υ_2 with eight modes being observed (Table 1). However, the weak feature at 8.604 eV, lying 1.535 eV from the (0–0) transition might also be adjudged to arise from 4 quantum modes related to the symmetric stretching υ_1 mode. Tanaka and co-workers [23] have observed strong evidence of resonance enhancement into this symmetric stretching mode. Thus, an alternative series in υ_1 may be assigned with an average energy spacing of ~0.384 eV implying that the normal mode description of vibrations is very powerful for the lowest lying excitations, with the possibility of strong Fermi resonance. We also conclude that the 8.658 eV peak is more likely to be a member of a υ_2' series (Table 1) rather than a Σ ($D_{\infty h}$) hot subband as suggested by Wang et al. [11].

5.2. Valence excitation in the energy range 8.5–10.0 eV

The energy positions and vibrational analysis of features observed in this absorption band correspond to $3sa_1 : \tilde{B}^1A_1 \leftarrow 3a_1 : \tilde{X}^1A_1$ and $3sa_1 : \tilde{C}^1A_1 \leftarrow 1b_1 : \tilde{X}^1A_1$ transitions (Fig. 3 and Table 2). This band is mainly dissociative producing $OH(\tilde{A}^2\Sigma^+) + H(^2S)$ products. This absorption band is rich in vibrational excitation which once again may be ascribed to υ_2 bending mode and the υ_1 symmetric stretching mode, the latter proposed here for the first time. Note that strong evidence of resonance enhancement into this symmetric stretching mode has been reported by Tanaka and co-workers [23]. The origin of the υ_2 bending mode and the υ_1 symmetric stretching mode lies at 8.658 eV (Table 2) despite the low intensity of this structure; since this band corresponds also to excitation to a linear component of the Renner–Teller splitting the origin has $\upsilon' = 1$ instead of υ_{00}. The energy spacing of υ_1' and υ_2' in the excited state are in good agreement to the energies found by Wang et al. [11]. However, $\Delta\upsilon_1'$ and $\Delta\upsilon_2'$ are almost in the ratio 1:4. Therefore, the normal mode description of vibrations is very powerful for the lowest lying excitations, with the

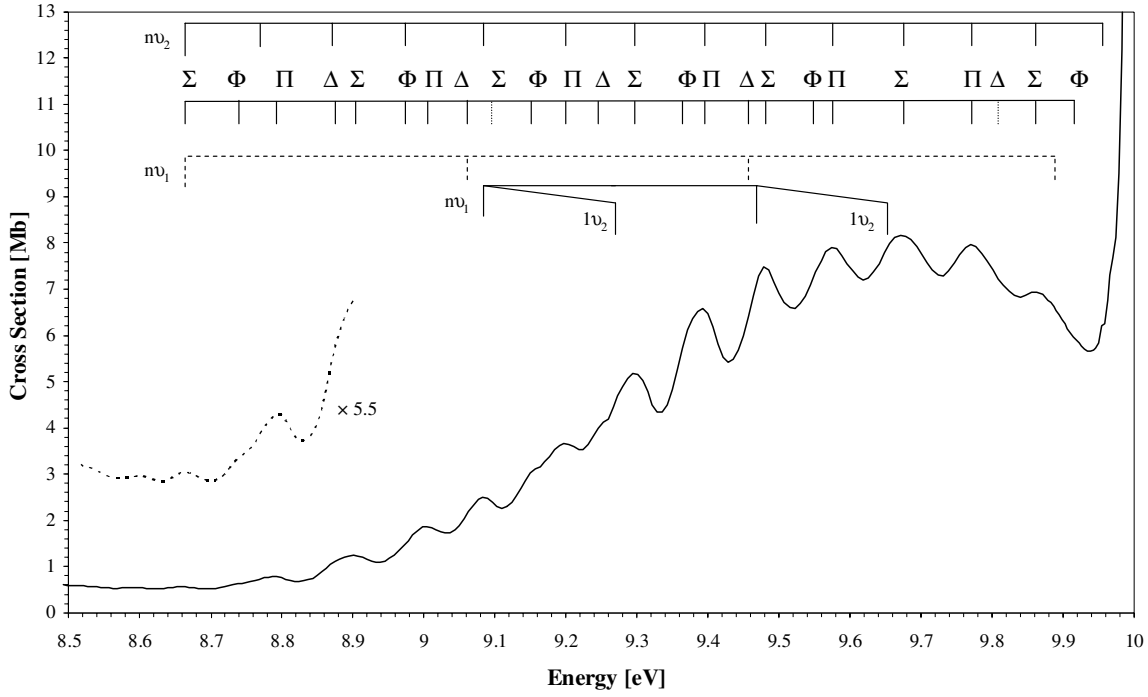

Fig. 3. H_2O photo-absorption spectrum from 8.5 to 10.0 eV with labelled vibrational series.

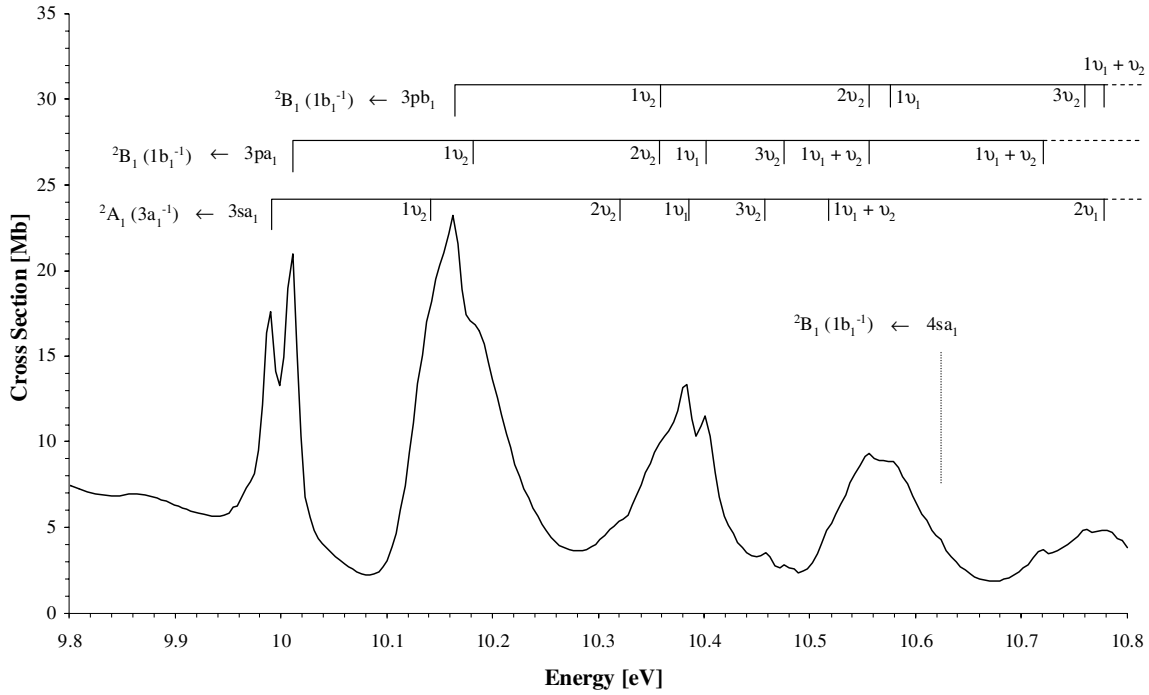

Fig. 4. H_2O photo-absorption spectrum from 9.8 to 10.8 eV with labelled Rydberg series and designated modes of vibrational excitation.

possibility of strong Fermi resonance, as observed in the previous band. Although the previous assignments by Wang et al. [11] suggest the activation of υ_2' , υ_1' should be considered when the broad nature of the peaks suggests a contribution of more than one mode being excited, or as in the present case it matches the position of some of the Renner–Teller Δ sub-band. It is noteworthy the two new proposed Φ assignments at 8.737 and 9.911 eV (Table 2).

The feature at 8.598 eV is tentatively assigned as a υ_2 hot band of the 8.658 eV $\Sigma(D_{\infty h})$ sub-band with an energy spacing of 0.060 eV, in agreement with the values obtained from Bell [10]; in the present assignments we have also decided to attribute the feature at 8.658 eV to the origin of the band, (0–0). The diffuse structure at 9.883 eV in Table 2, is tentatively assigned to $4\upsilon_1$ despite the higher energy spacing from the $3\upsilon_1$.

5.3. Valence excitation in the energy range 9.9–10.8 eV

This energy region is dominated by series of sharp peaks superimposed on a relative low background (Fig. 4). Valence excitation in this energy region is attributed to the $nsa_1/4a_1 : \tilde{C}^1A_1 \leftarrow 1b_1 : \tilde{X}^1A_1$ and $npa_1/npb_1 : \tilde{C}^1A_1 \leftarrow 1b_1 : \tilde{X}^1A_1$ transitions [22]. The $\tilde{C}$ state is bonding in the H–OH co-ordinate. However, at sufficiently large HOH angles and H–OH distances (<1.6 Å), a water molecule in the Renner–Teller component $\tilde{B}^1A_1$ of the $^1\Pi_u$ state of linear H_2O can reach the $\tilde{A}^1B_1$ state via a linear Renner–Teller intersection, the coupling of which has been reported to be Coriolis in nature [28]. Since the $\tilde{A}$ state is strongly antibonding, correlating with $OH(\tilde{X}^2\Pi) + H(^2S)$, the direct transition $\tilde{B}^1A_1 \leftarrow \tilde{X}^1A_1$ is also possible via a conical intersection at these H–OH bond distances. Kuge and Kleinermanns [28] report that ~10% of the photo-excited $\tilde{C}$ state does not reach the $\tilde{A}$ or $\tilde{X}$ states but dissociate from the $\tilde{B}^1A_1$ through the adiabatically correlated $OH(\tilde{A}^2\Sigma^+) + H(^2S)$ products.

The absolute oscillator strengths in this energy band have been carefully obtained by Chan et al. [20] and a detailed analysis and assignments have been proposed. Vibrational excitation of υ_1 and υ_2 were reported, but due to the high resolution achieved in the present work, has been possible the identification on new structures (Fig. 4, Tables 3 and 4).

However, the cross-section in this region is dominated by a series of sharp transitions which are attributable to Rydberg transitions (Tables 3 and 4). It should be noted that the peak at 9.967 eV remains unassigned.

5.4. Rydberg series

The cross-section above 9 eV consists of a series of sharp Rydberg peaks progressing up to the two lowest ionisation limits, 12.621 and 14.730 eV (Figs. 1 and 4). The peak positions, E_n, must fit the Rydberg formula: $E_n = E_i - R/(n-\delta)^2$, where E_i is the ionisation energy, n is the principal quantum number of the Rydberg orbital of energy E_n, R is one Rydberg and δ the quantum defect resulting from the penetration of the Rydberg orbital into the core. Very few vibrational excitation bands in the Rydberg region have been identified in previous absorption spectra, hence we present a detailed analysis of the structure we observed and several new assignments are proposed.

The $\tilde{A}^1B_1$ and $\tilde{B}^1A_1$ states mark the beginning of a series of bent-linear Rydberg states, closely linked by a Renner–Teller mixing character. As far as this vibronic–electronic

Table 2
Energy positions and vibrational analysis of features observed in the second absorption band (8.5–10.0 eV) of H_2O (energies in eV)

This work								Wang et al. [11]		
Energy	Sub-band ($D_{\infty h}$)	Assignment	ΔE (υ_2')	Assignment	ΔE (υ_1')	Assignment	ΔE (υ_1')	Energy	Assignment	
8.598		2_1^0(?)	0.060					8.623		
8.658	Σ	$\upsilon_{00}/1\upsilon_2$	–			$1\upsilon_1$	–	8.659	$1\upsilon_2$	
8.737	Φ							–		
8.775		$2\upsilon_2$	0.111					–		
8.793	Π							8.789	$2\upsilon_2$	
8.875	Δ	$3\upsilon_2$						8.794		
8.901	Σ		0.100					8.904	$3\upsilon_2$	
8.978	Φ	$4\upsilon_2$	0.103					8.966		
9.004	Π							9.008	$4\upsilon_2$	
9.063 (s)	Δ					$2\upsilon_1$	0.405	–		
9.083		$5\upsilon_2$	0.105	υ_{00}	–			9.086		υ_{00}
9.096 (d)	Σ							9.104	$5\upsilon_2$	
9.150	Φ							9.161		
9.198	Π	$6\upsilon_2$	0.115					9.200	$6\upsilon_2$	
9.245	Δ							9.247		
9.273								9.252		$1\upsilon_2$
9.294	Σ	$7\upsilon_2$	0.096					9.297	$7\upsilon_2$	
9.364	Φ							9.358		
9.393	Π	$8\upsilon_2$	0.099					9.394	$8\upsilon_2$	
9.464 (s)	Δ					$3\upsilon_1$	0.401	–		
9.472				$1\upsilon_1$	0.389			9.482		$1\upsilon_1$
9.479	Σ	$9\upsilon_2$	0.086					9.489	$9\upsilon_2$	
9.552	Φ							9.542		
9.574	Π	$10\upsilon_2$	0.095					9.584	$10\upsilon_2$	
9.656				$1\upsilon_1 + 1\upsilon_2$	–			9.661		$1\upsilon_1 + 1\upsilon_2$
9.671	Σ	$11\upsilon_2$	0.097					9.678	$11\upsilon_2$	
9.770	Π	$12\upsilon_2$	0.099					9.771	$12\upsilon_2$	
9.809 (d)	Δ							9.808		
9.864	Σ	$13\upsilon_2$	0.094					9.865	$13\upsilon_2$	
9.883 (s)						$4\upsilon_1$ (?)	0.419	–		
9.911 (d)	Φ							–		
9.955		$14\upsilon_2$	0.091					–		

(d) means diffuse structure; (s) means shoulder; (?) means uncertainty.

Table 3
Energy values, quantum defect and assignment of the Rydberg series converging to the ionic electronic ground state $\tilde{X}^2B_1(1b_1^{-1})$ of H_2O (energies in eV)

Energy	Quantum defect	Assignment	ΔE (υ_2')	ΔE (υ_1')
7.464	1.38	$3sa_1$	–	–
10.624	1.39	$4sa_1$	–	–
10.011	0.72	$3pa_1$	–	–
10.179 (s)	–	$3pa_1 + 1\upsilon_2$	0.168	–
10.354 (s)	–	$3pa_1 + 2\upsilon_2$	0.175	–
10.401	–	$3pa_1 + 1\upsilon_1$	–	0.390
10.476	–	$3pa_1 + 3\upsilon_2$	0.156	–
10.556	–	$3pa_1 + 1\upsilon_1 + 1\upsilon_2$	0.155	–
10.721	–	$3pa_1 + 1\upsilon_1 + 2\upsilon_2$	0.165	–
10.163	0.65	$3pb_1$	–	–
10.360	–	$3pb_1 + 1\upsilon_2$	0.197	–
10.556	–	$3pb_1 + 2\upsilon_2$	0.196	–
10.574	–	$3pb_1 + 1\upsilon_1$	–	0.411
10.763	–	$3pb_1 + 3\upsilon_2$	0.207	–
10.777	–	$3pb_1 + 1\upsilon_1 + 1\upsilon_2$	0.203	–

(s) means shoulder.

Table 4
Energy values, quantum defect and assignment of the Rydberg series converging to the ionic electronic first excited state $\tilde{A}^2A_1(3a_1^{-1})$ of H_2O (energies in eV)

Energy	Quantum defect	Assignment	ΔE (υ_2')	ΔE (υ_1')
9.991	1.31	$3sa_1$	–	–
10.142	–	$3sa_1 + 1\upsilon_2$	0.151	–
10.320 (s)	–	$3sa_1 + 2\upsilon_2$	0.178	–
10.384	–	$3sa_1 + 1\upsilon_1$	–	0.393
10.458	–	$3sa_1 + 3\upsilon_2$	0.138	–
10.516 (s)	–	$3sa_1 + 1\upsilon_1 + 1\upsilon_2$	0.156	–
10.777	–	$3sa_1 + 2\upsilon_1$	–	0.393

(s) means shoulder.

coupling affecting the whole corresponding series is concerned, electronic couplings between lower linear states make the interpretation of the stability of the Rydberg states very complex [21].

The first two intense bands peaking at 9.991 and 10.011 eV have been identified to correspond to the first strong resonance bands [8]. The energy separation of

20 meV is in agreement with the reported value from Price [8]. Two less intense bands are observed at 10.384 and 10.401 eV, ~0.390 eV above the former corresponding to the excitation in υ_1. The excited state energy values obtained from Watanabe and Jursa [9] for υ_1' and υ_2' are in close agreement to the values obtained for the assignments proposed in Tables 3 and 4.

The calculated excitation series converging to the $^2B_1(1b_1^{-1})$ and $^2A_1(3a_1^{-1})$ ionic limits include contributions from Rydberg and $4a_1$ valence like orbitals [22]. The promotion of a $3a_1$ electron gives rise to two 3s states, which have a valence character at extended H–OH bond length, giving rise to broad absorption features associated with $3sa_1 \leftarrow 1b_1(\tilde{A}^1B_1 \leftarrow \tilde{X}^1A_1)$ and the $3sa_1 \leftarrow 3a_1(\tilde{B}^1A_1 \leftarrow \tilde{X}^1A_1)$ transitions peaking at 7.464 and 9.991 eV, respectively.

5.4.1. Rydberg series converging to the lowest ionic ground state, $^2B_1(1b_1^{-1})$

The first term of a nsa_1 series was reported by Price [8] to be at ~7.750 eV and is here found at 7.464 eV (Table 3, Fig. 2), with a quantum defect $\delta = 1.38$; this ns quantum defect is in agreement with Gürtler et al. [12] and Diercksen et al. [22]. Due to the strong pre-dissociative character of the $\tilde{A}^1B_1$ band, this feature is, however, very weak. It corresponds to the $3sa_1\tilde{A}^1B_1 \leftarrow 1b_1:\tilde{X}^1A_1$ transition and is known to photo-dissociate into OH and H radical fragments. Diercksen et al. [22] suggested that a diabatic dissociative surface associated with the $1b_1^{-1}4a_1(\gamma^*)$ configuration may cross the $1b_1 \rightarrow nsa_1$ Rydberg series in the vicinity of the ground-state vertical Franck–Condon region. The 4*s* term appears at 10.624 eV with a quantum defect of 1.39.

The $3pa_1/3pb_1$, υ_1' and υ_2' excitation energies are in good agreement with the values obtained from the work of Bell [10], Ishiguro et al. [13] and Gürtler et al. [12], (~0.394/0.405 eV) and (~0.175/0.203 eV), respectively. The first member of the $npa_1\tilde{C}^1B_1 \leftarrow 1b_1:\tilde{X}^1A_1$ ($n = 3$) Rydberg series is proposed to lie at 10.011 eV, with a quantum defect $\delta = 0.72$ (Table 3) in contrast to the previously reported value of ~9.995 eV [8,12].

The first member of the $npb_1\tilde{C}^1B_1 \leftarrow 1b_1:\tilde{X}^1A_1$ series ($n = 3$) is proposed to lie at 10.163 eV (Fig. 4) compared to the previously reported values of ~10.171 eV [12]. The strongest band in the progression at 10.163 eV is accompanied by a much weaker band at 10.574, with an energy spacing of 0.411 eV, assigned to the excitation of υ_1' in good agreement with [8].

Vibrational structure associated with the bending υ_2' and symmetric stretching υ_1' modes are identified in all the Rydberg series (Table 3). The excitation energies of these modes are in agreement with Bell [10].

5.4.2. Rydberg series converging to the second ionic ground state, $^2A_1(3a_1^{-1})$

The first member of the $nsa_1\tilde{C}^1B_1 \leftarrow 3a_1:\tilde{X}^1A_1$ Rydberg series is found at 9.991 eV with a quantum defect $\delta = 1.31$ (Table 4, Fig. 4) compared with the previous reported values of ~9.850 eV (with a quantum defect of $\delta = 1.33$) [12]. The $3a_1 \rightarrow nsa_1$ contains a $3sa_1/4a_1$ partially intravalence resonance member at its origin (9.991 eV) and the other members are broader than the other bands in the spectrum, which can be attributed to interaction with an underlying dissociative valence state.

Vibrational structure associated with the bending υ_2' and symmetric stretching υ_1' modes are identified for the Rydberg series (Table 3). The excitation energies of these modes are once again in agreement with those reported by Bell [10].

The broad structure located at 9.865 eV, previously assigned as a member of a υ_2' series (Table 2) [12,22], is now ascribed to a valence/Rydberg mixing character and can be assigned to the $3a_1 \rightarrow ns$ Rydberg series (with a quantum defect of $\delta = 1.33$).

6. Conclusions

The present absolute cross-section for H_2O in the energy region 6–11 eV are, we believe, the highest resolution set of VUV data yet reported. New vibrational assignments have been proposed for the fine structure observed in all the photo-absorption bands. The large change in geometry involved in going from the bent ground state to quasilinear state, long vibrational progressions in the excited states were observed.

The 7.447 eV state is $^1B_1$ bonding and contains a considerable $4a_1$ intravalence component. It has therefore, been described as $4a_1/3sa_1$: $^1B_1$. The 9.671 eV state is a 3s, $^1A_1$ state, linear in nature, exhibiting strong Renner–Teller vibronic characteristics. The $4a_1$ (γ^*) virtual (valence) orbital is found to contribute mainly to the nsa_1 series, particularly to the $1b_1 \rightarrow 3sa_1/4a_1$ and $3a_1 \rightarrow 3sa_1/4a_1$ resonance members, leading to broad photo-dissociation bands and giving rise to a mixed valence/Rydberg character in the energy region.

Acknowledgements

R.M. acknowledges the support from the EU/ESF COST Action P9 and R.P. the financial support from the EIPAM network, ESF, for the short term scientific mission to Liège, Belgium. P.L.V. acknowledges the honorary research fellow position at University College London and a visiting fellowship position at CEMOS, The Open University, UK and together with N.J.M. the support from the British Council for the Portuguese–English joint collaboration. P.L.V. and G.G. are also thankful to the GRICES/CSIC Portuguese–Spanish joint research collaboration. M.J.H.F. acknowledges the FNRS for research position. Professor Jacques Delwiche of the Université de Liège, Belgium is also acknowledged for his valuable advices. The authors wish to acknowledge the beam time at the ISA synchrotron facility, University of Aarhus, Denmark, and the support from the European Commission – Access to Research Infrastructure Action of the Improving Human Potential Programme, contract number RII3-CT-2004-506008.

References

[1] B. Nisini, Science 290 (2000) 1513.
[2] F.W. Taylor, Rep. Prog. Phys. 65 (2002) 1.
[3] W.M. Becker, L.J. Kleinsmith, J. Hardin, The World of the Cell, fifth edn., Benjamin Cummings, San Francisco, 2003.
[4] L. Sanche, Mass Spectrom. Rev. 21 (2003) 349.
[5] H. Abdoul-Carime, S. Gohlke, E. Illenberger, Phys. Rev. Lett. 92 (2004) 168103.
[6] F. Martin, P.D. Burrow, Z.L. Cai, P. Cloutier, D. Hunting, L. Sanche, Phys. Rev. Lett. 93 (2004) 068101.
[7] Y. Itikawa, N.J. Mason, J. Phys. Chem. Ref. Data 34 (2005) 1 (and references therein).
[8] W.C. Price, J. Chem. Phys. 4 (1936) 147.
[9] K. Watanabe, A.S. Jursa, J. Chem. Phys. 41 (1964) 1650.
[10] S. Bell, J. Mol. Spectrosc. 16 (1965) 205.
[11] H.-T. Wang, W.S. Felps, S.P. McGlynn, J. Chem. Phys. 67 (1977) 2614.
[12] P. Gürtler, V. Saile, E.E. Koch, Chem. Phys. Lett. 51 (1977) 386.
[13] E. Ishiguro, M. Sasanuma, H. Masuko, Y. Morioka, M. Nakamura, J. Phys. B 11 (1978) 993.
[14] K. Yoshino, J.R. Esmond, W.H. Parkinson, K. Ito, T. Matsui, Chem. Phys. 211 (1996) 387.
[15] B.D. Bursulaya, J. Jeon, C.-N. Yang, H.J. Kim, J. Phys. Chem. A 104 (2000) 45.
[16] C.-Y. Chung, E.P. Chew, B.-M. Cheng, M. Bahou, Y.-P. Lee, Nucl. Instrum. Methods Phys. Res. A 467–468 (2001) 1572.
[17] R.K. Vatsa, H.-R. Volpp, Chem. Phys. Lett. 340 (2001) 289.
[18] W.H. Parkinson, K. Yoshino, Chem. Phys. 294 (2003) 31.
[19] L.C. Lee, M. Suto, Chem. Phys. 110 (1986) 161.
[20] W.F. Chan, G. Cooper, C.E. Brion, Chem. Phys. 178 (1993) 387.
[21] J.-H. Fillion, J. Ruiz, X.-F. Yang, M. Castillejo, F. Rostas, J.-L. Lemaire, J. Chem. Phys. 120 (2004) 6531.
[22] G.H.F. Diercksen, W.P. Kraemer, T.N. Rescigno, C.F. Bender, B.V. McKoy, S.R. Langhoff, P.W. Langhoff, J. Chem. Phys. 76 (1982) 1043.
[23] C. Makochekanwa, R. Katija, H. Kato, M. Kitajima, H. Cho, M. Kimura, H. Tanaka, J. Chem. Phys. 122 (2005) 014314.
[24] T. ShimanouchiTables of Molecular Vibrational Frequencies Consolidated, vol. I, National Bureau of Standards, 1972, pp. 1–160.
[25] J.H.D. Eland, Photoelectron Spectroscopy, Butterworths, London, 1984.
[26] S.G. Lias, Ionization Energy Evaluation, in: P.J. Linstrom, W.G. Mallard (Eds.), NIST Chemistry WebBook, NIST Standard Reference Database Number 69, June 2005, National Institute of Standards and Technology, Gaithersburg MD, 20899. Available from: <http://webbook.nist.gov>.
[27] S. Eden, P. Limão-Vieira, S.V. Hoffmann, N.J. Mason, Chem. Phys., in press.
[28] H.-H. Kuge, K. Kleinermanns, J. Chem. Phys. 90 (1989) 46.